Journal of
Composites Science

MDPI

Article

Enhanced Photocatalytic Degradation of Amoxicillin with Mn-Doped Cu_2O under Sunlight Irradiation

Yohannes Teklemariam Gaim [1,*], Simachew Mekides Yimanuh [1] and Zaid Girmay Kidanu [2]

[1] Department of Chemistry, College of Natural and Computational Sciences, Werabe University, Werabe P.O. Box 46, Ethiopia
[2] Department of Biology, College of Natural and Computational Sciences, Werabe University, Werabe P.O. Box 46, Ethiopia
* Correspondence: yohannesteklemariam1@gmail.com; Tel.: +251-932034081

Abstract: In this work, we report the synthesis of Mn-doped Cu_2O nanoparticles using aloe vera leaves extract. X-ray diffraction data revealed that the Mn-doped Cu_2O crystals have a cubic crystal structure. The surface morphology of the as-synthesized catalyst indicated truncated octahedral and spherical-like shapes. The photocatalytic activity of the catalyst is efficient at pH 9, initial concentration of amoxicillin 15 mg/L, and photocatalyst dosage 1 g/L under sunlight irradiation. 92% of amoxicillin was degraded in the presence of Mn-doped Cu_2O. The enhancement in photocatalytic performance is due to the incorporation of Mn, which delays the rapid recombination rate by trapping the photogenerated electron. Therefore, Mn-doped Cu_2O could remove pharmaceuticals from pharmaceutical factory and hospital wastes.

Keywords: aloe vera; amoxicillin; photocatalyst; degradation

Citation: Gaim, Y.T.; Yimanuh, S.M.; Kidanu, Z.G. Enhanced Photocatalytic Degradation of Amoxicillin with Mn-Doped Cu_2O under Sunlight Irradiation. *J. Compos. Sci.* **2022**, *6*, 317. https://doi.org/10.3390/jcs6100317

Academic Editors: Francesco Tornabene and Thanasis Triantafillou

Received: 2 September 2022
Accepted: 10 October 2022
Published: 17 October 2022

1. Introduction

The increment of pollutants in water system has become one of the environmental problems which needs to be addressed by environmental protection agencies. Pharmaceuticals, mainly antibiotics, are part of the various emerging contaminants that have been identified in diverse water matrices. Several studies have presented that most antibiotics are not digested well by humans and animals. Around 25–75% of these drugs consumed by the living organisms form part of the excrement and urine [1–3]. These antibiotics reach the water bodies and the environment through several means, for example waste water from hospitals, pharmaceutical industry, and from human and animal waste deposits [4]. The contamination of environment, especially water bodies and soil, with these antibiotics is of concern because of their highly persistent, toxicity to aquatic life, acute and chronic toxicity effect on humans and animals, and propagation of antibiotic resistant microorganism [5,6].

Amoxicillin (AMX) is one of the most widely used antibiotics to treat human infections [7,8]. Several reports have shown that over 80 percent of orally administered amoxicillin in humans is excreted through urine after 2 hour of ingestion [6,9]. Currently, the concentration of amoxicillin present in hospital [10], industrial, and domestic [11,12] wastewaters has been reported within ng/L to mg/L range.

Numerous techniques have been used to remove antibiotics from different mediums, such as adsorption, advanced oxidation processes, and membrane filtration [13,14]. Among other techniques, advanced oxidation processes (AOPs) have been found to be the most effective for the removal of these pharmaceuticals. This technique has hydroxyl radical to oxidize the organic compounds into harmless products, and the capability of operating at ambient conditions and utilize sunlight as the source of energy [4,15]. Photocatalysis is one of the emerging AOP techniques which utilizes nanometer-sized catalyst and light as the energy source to activate chemical reactions [16,17].

Photocatalysis is widely used for the degradation of organic pollutants. The development of new materials, which are low-cost, environmentally friendly, and present long-term durability has attracted great attention. Recently, ZnO and TiO_2 photocatalyst have been significantly investigated in advanced oxidation of pollutants [18]. These metal oxide semiconductors absorb small amount of sunlight because their bandgap energy is large (3.0–3.2 eV). They cannot harvest sunlight as a source of energy. Hence, production of catalysts which can efficiently utilize sunlight is a fundamental scientific research area.

Cuprous oxide (Cu_2O) is a p-type of semiconductor with a direct band gap of 2.0–2.2 eV [19]. Cu_2O is unique in magnetic and optical properties, applicable in solar energy conversion, electrode material, gas sensor, and visible light-driven photocatalyst of organic contaminants [20]. Cupper (I) oxide has been widely used as a photocatalyst due to its advantages such as nontoxicity, easy availability, absorption of large fraction of visible light [21–23]. However, due to the rapid recombination of photo generated electrons and holes, pure cuprous oxide photocatalyst is seriously restricted in practical application. Hence, inhibition of the electrons and holes recombination is important to enhance photocatalytic activity of cuprous oxide. To overcome the electron-hole recombination and enhance the photocatalytic performance of the material, different techniques can be used such as doping [24], composite modification [25,26], or the formation of heterojunction [27,28]. According to [29], the photo-induced electrons in the conduction band of the cuprous oxide can be transferred to the metal which can serve as electron sink. Consequently, the lifetime of the electron can be increased, and the photocatalytic performance can be enhanced. The use of plant extracts in the synthesis of nanoparticles enables the production of large quantities of nanoparticles and can act both as reducing and stabilizing agents [30,31].

Green synthesis is a method used to synthesize nanoparticles from plant extract and microorganisms. Currently, this method has attracted significant attention as it has numerous advantages such as simplicity, cost-effectiveness, non-toxic, production of large quantities, and being environmental friendly. Plant extracts play important roles of being a reducing, stabilizing, and size controlling agent in the preparation of nanoparticles. In the chemical method, toxic chemicals are used for the production of nanoparticle. The toxic chemical species may adsorb on the surface of nanoparticles, thus affecting the environment. Moreover, the reducing and stabilizing agents used in chemical methods are expensive. Therefore, green synthesis has attained special attention for the production of different nanoparticles [32,33].

Up to the present time, researchers have investigated different photocatalysts which can degrade amoxicillin. Photocatalytic degradation of amoxicillin was studied by [34] using TiO_2 photocatalyst under UV irradiation. According to the authors, 60% of amoxicillin was degraded within 300 min of irradiation. Rani et al. (2021) examined the photocatalytic degradation of amoxicillin using TiO_2-SiO_2 composites. 88% of amoxicillin was degraded in 150 min under UV light illumination [35]. Photocatalytic decomposition of amoxicillin was investigated by Mohammadi et al. (2012) using Sn/TiO_2. According to the authors, Sn/TiO_2 nanoparticles showed good activity in the mineralization of amoxicillin under UV light [36]. Olama et al. (2018) investigated the removal of amoxicillin from aqueous solution using TiO_2/UV-C doped with trivalent iron. 99% of amoxicillin was removed by the catalyst under UV irradiation. The researchers investigated the photocatalytic removal of amoxicillin using ultraviolet radiation as a source of energy. As sunlight is a natural energy source, using sunlight as source of energy in photocatalysis is important for saving our energy. In the present study, we used sunlight as a source of energy for photocatalytic degradation of amoxicillin.

In this work, Mn-doped Cu_2O photocatalyst were fabricated via green synthesis method from aloe vera leaf extract. The structural, morphological, and optical properties of the nanoparticles were analyzed. Moreover, the photocatalytic performance of the nanoparticle was investigated in photocatalytic degradation of amoxicillin under sunlight irradiation.

2. Materials and Methods

2.1. Materials

The following chemicals were used throughout the study. Manganese sulphate monohydrate ($MnSO_4.H_2O$, Sigma-Aldrich, St. Loui, MI, USA), copper sulfate pentahydrate ($CuSO_4.5H_2O$, Sigma-Aldrich), sodium hydroxide (NaOH, Sigma-Aldrich), ethanol (C_2H_6O, Sigma-Aldrich), and distilled water. All the chemicals were analytical grade and used without further purification.

2.2. Synthesis

2.2.1. Preparation of Aloe Vera Leaves Extract

Aloe vera leaves were collected, washed thoroughly using distilled water and cut into fine pieces. About 25 g (0.25 g/mL) of these pieces was added into 100 mL distilled water and boiled for 2 h at 90 °C. The extract was filtered, and finally the filtrate was stored in 5 °C for synthesis of nanoparticle [37].

2.2.2. Synthesis of Mn-Doped Cu_2O Nanoparticles

The Mn-doped Cu_2O nanoparticles were synthesized from $CuSO_4.5H_2O$ and $MnSO_4.H_2O$ as precursors through eco-friendly method using aloe vera leaves extract. To prepare Mn-doped cuprous oxide nanoparticles, 1.9 mmole of $CuSO_4.5H_2O$ were dissolved in 100 mL of aloe vera aqueous extract. Afterwards, 0.1 mmole of $MnSO_4.H_2O$ was added to the solution under stirring. Then, 40 mL of 2M NaOH solution was added drop by drop to the above solution and kept at 130 °C under vigorous stirring. After 25 min, orange colored precipitate was formed. Thereafter, the precipitate was collected by centrifugation and washed using ethanol and water three times each. Finally, the product was dried at 90 °C for 7 h [38,39]. In order to compare with undoped Cu_2O nanoparticle, brick red colored pure Cu_2O was also synthesized using similar method in Mn-doped Cu_2O nanoparticle except adding $MnSO_4 \cdot H_2O$ into the solution.

2.3. Characterization Techniques

Crystal structure and average crystallite size of the synthesized nanoparticles were analyzed using X-ray diffractometer (shimadzu XRD-7000). XRD fitted with a copper target to produce a Cu K radiation (λ = 0.15406 nm) was used. The accelerating voltage and functional current were set at 40 kV and 30 mA, respectively. Operation of the instrument was in step time of 0.4 second and degree of 0.02° for the range of 10° to 80°. Identification of the types of the materials from their XRD peak was in terms of the position of the 2θ lines with respect to the relative intensity of these lines. The surface morphological structures of the nanoparticles were studied using scanning electron microscopy (SEM), JEOL JSM-5610 (JEOL, Ltd., Akishima, Tokyo, Japan) equipped with an Everhart-Thornley detector. The optical property of the photocatalyst was recorded using UV-Vis diffuse reflectance spectrometer on diffuse reflectance in a wavelength range of 220–800 nm.

2.4. Photocatalysis Experiments

The photocatalytic degradation experiments were conducted by direct sunlight illumination on sunny days from 10:30 AM to 2:30 PM when fluctuation of solar intensity was negligible [40]. Average intensity of the sunlight during degradation experiments was 900 W/m^2. Aqueous solution of amoxicillin was prepared first by the addition of 25 mg of amoxicillin into 1L deionized water (25 mg/L aqueous solution of amoxicillin). In the photocatalytic degradation experiment, effect of operational parameters including initial pH (3–11), catalyst dosage (0.5–2.5 g/L), and initial concentration of amoxicillin (5-50 mg/L) were investigated. These parameters were optimized by preparing synthetic solution of amoxicillin in laboratory. The experiment was carried out at a temperature range of 24–26 °C and the solution pH was adjusted to the desired level using 1M HCl and 1M NaOH. Typically, the photocatalytic degradation experiment was performed as follows: 0.1 g of the photocatalyst was added/ dispersed into 100 mL of 15 mg/L aqueous

solution of amoxicillin. Then, the suspension containing amoxicillin and photocatalyst was stirred in dark for 1 hr to establish adsorption/desorption equilibrium before irradiating to sunlight. Afterwards, the suspension was irradiated to sunlight and photocatalytic reaction time was started. The suspension was sampled after appropriate time of irradiation. Finally, the degraded sample was centrifuged and filtered to eliminate any suspended solids before measuring absorption. The filtrate of each degraded sample was assessed for amoxicillin concentration after conducting absorbance reading at 280 nm using UV-Vis spectrophotometer. The percentage degradation (degradation efficiency) of amoxicillin was determined by the following calculation.

$$\% \text{ degradation} = \frac{\text{Co} - \text{Ce}}{\text{Co}} \times 100$$

where Co is initial concentration of amoxicillin and Ce is concentration of amoxicillin at each time interval [5,41].

3. Results and Discussion

3.1. XRD Analysis

Figure 1a,b displays the diffraction patterns of pure and Mn-doped Cu_2O nanoparticles. The diffraction peaks in the XRD patterns of Cu_2O nanoparticle at 2θ value of 29.60°, 36.47°, 42.36°, 52.45°, 61.44°, 73.60°, and 77.47° corresponds to (110), (111), (200), (211), (220), (311), and (222) crystal planes of cubic structure of cuprous oxide. In the XRD pattern of Mn-Cu_2O nanoparticle, the peaks located at: 29.70°, 36.56°, 42.46°, 52.56°, 61.55°, 73.70°, and 77.58° are also assigned to the (110), (111), (200), (211), (220), (311), and (222) crystal planes of cubic cuprite structure of the synthesized nanoparticle [42,43]. The obtained pattern was found in accordance with the standard pattern of Cu_2O (JCPDS No.00-005-0667). The XRD patterns of Mn-doped Cu_2O exhibited all peaks of the pure Cu_2O with slight shift which showed successful doping of Mn. The peaks are sharp which indicated high crystallinity of the prepared nanomaterial. X-ray diffraction measurement showed no existence of secondary phase in the Cu_2O lattice structure. The Mn ions are incorporated in Cu_2O lattice. There is no detection of impurity phase ascribed to manganese oxide which indicated that complete doping of Mn^{2+} in to the Cu_2O crystal lattice [44].

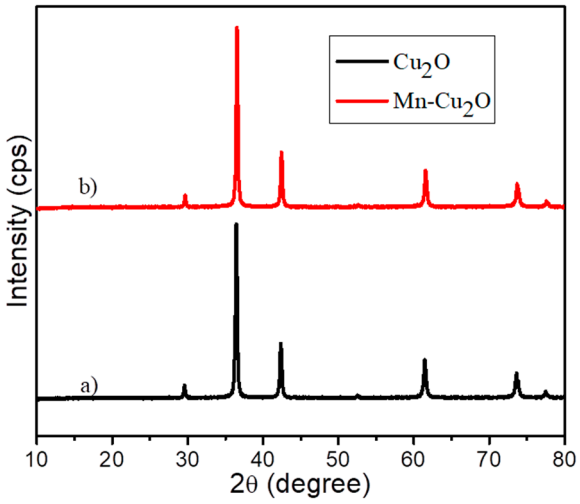

Figure 1. (**a**) XRD pattern of Cu_2O (**b**) Mn-Cu_2O nanoparticles.

Average crystallite sizes of the nanoparticles were estimated from the intensive diffraction peak using the Scherrer equation written below.

$$D = \frac{0.9\lambda}{\beta \cos\theta}$$

where D is the average crystallite size, λ the X-ray wavelength, θ the Bragg diffraction angle, and β is the full width at half maximum (FWHM) intensity of the peak in radian. The average crystallite size was found to be 37.32 nm and 39.27 nm for bare Cu_2O and Mn-doped Cu_2O respectively as shown in Table 1.

Table 1. Crystalline size of undoped and Mn-doped Cu_2O nanoparticles.

Nanoparticles	2θ (Deg)	FWHM (Radian)	Crystallite Size (nm)
pure Cu_2O	36.467	0.004551	37.32
Mn-doped Cu_2O	36.562	0.004188	39.27

3.2. Surface Morphology Analysis

The morphology of Cu_2O and Mn-doped Cu_2O nanoparticles was studied by scanning electron microscopy (SEM), as shown in Figure 2a,b. It was observed that the morphologies of pure and Mn-doped Cu_2O nanoparticles are homogeneously distributed octahedral and truncated octahedral respectively, as reported in [45,46]. Moreover, sphere like particles were observed in the morphology of Mn-doped Cu_2O, which is in agreement with Kerour et al. [38].

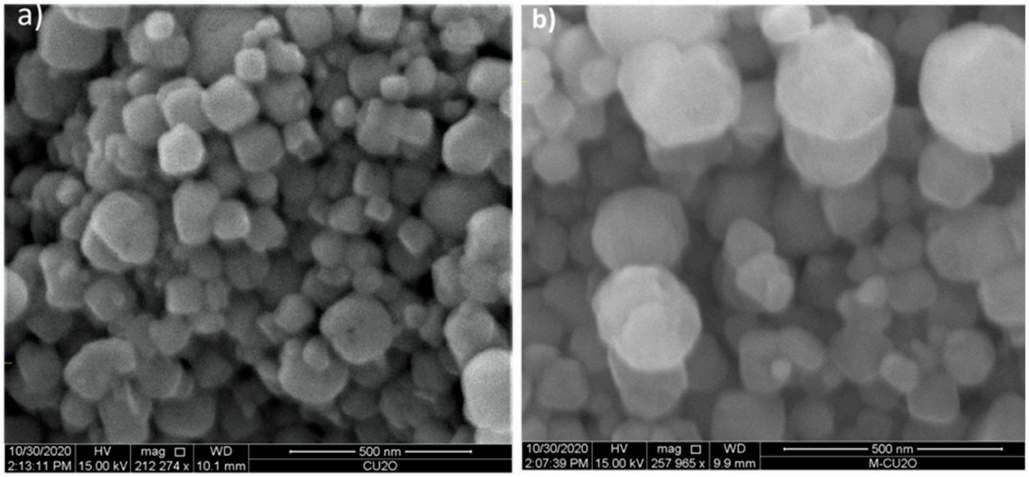

Figure 2. SEM images of (**a**) Cu_2O and (**b**) Mn-doped Cu_2O nanoparticles.

3.3. Optical Property Analysis

Absorption property of materials is a measure of the electronic excitation between valence and conduction bands of these materials, and notifies their bandgap energy (Eg). The optical absorption spectra of Cu_2O and Mn-doped Cu_2O nanoparticles are given in Figure 3a. To estimate the bandgap energy value of the nanoparticles, their absorption wavelength (λ) was measured by extrapolating downward slopes to cross the X-axis as determined by Norouzi et al. [47]. Absorption wavelength values of the as-synthesized Cu_2O and Mn-doped Cu_2O nanoparticles were found to be 539 and 564 nm, respectively. This demonstrated that Mn doping in Cu_2O shifted the absorption edge to longer wavelengths (red shift) which significantly improved the optical property of Cu_2O nanoparticle. This implies that the visible light harvesting capability of Cu_2O significantly increased, and notably promoted electron and hole separation which might increase active sites. The band gap energy of the nanoparticles was estimated from the intercepts of the tangents to the $(\alpha h\nu)^2$ versus $(h\nu)$ plots, where α is the absorption coefficient, ν is frequency, and h is Plank's constant [48–50]. The band gap energy values found for pure Cu_2O and Mn-Cu_2O nanoparticles were 2.3 eV and 2.2 eV, respectively, as displayed in Figure 3b. The existence of crystal defects and substoichiometry usually results in red-shift in band gap. The defects create certain states in the energy gap which can absorb sub-bandgap photons, thus causing artifacts and features that can be interpreted as a smaller bandgap compared to the real bandgap [51,52]. This confirmed Mn doping in Cu_2O creates more defect sites. Therefore, the optical absorption edge of nano-sized Mn-doped Cu_2O

absorbs more visible light than undoped Cu_2O nanoparticles. Table 2 depicts the absorption edge and band gap energy of the prepared photocatalysts.

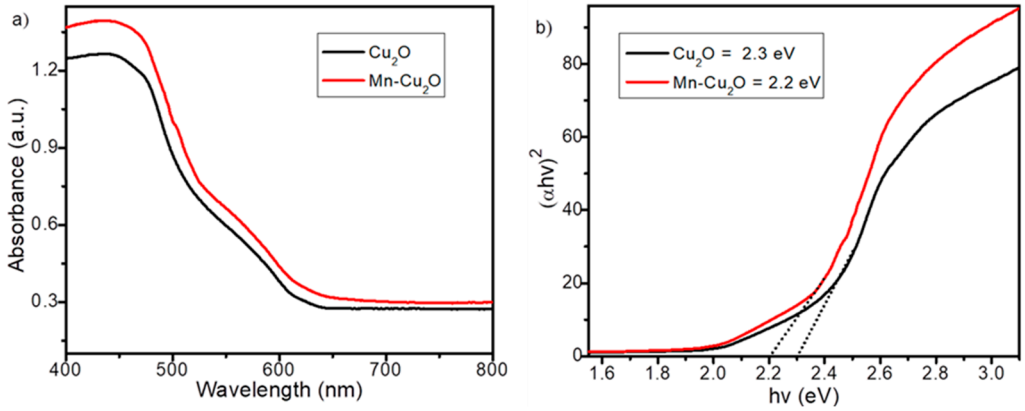

Figure 3. (**a**) Absorption spectra (**b**) $(\alpha h\nu)^2$ vs $(h\nu)$ plots of the nanoparticles.

Table 2. Absorption edge and band gap energy of undoped and Mn-doped Cu_2O nanoparticles.

Nanoparticle	Absorption Wavelength (nm)	Bandgap Energy (eV)
Undoped Cu_2O	539	2.3
Mn-doped Cu_2O	564	2.2

3.4. Photocatalytic Degradation of Amoxicillin

3.4.1. Effect of pH

pH is an essential factor in the removal efficiency of many organic pollutants. Figure 4 illustrates the effect of pH on the removal efficiency of amoxicillin by Mn-Cu_2O nanoparticle. To determine the effect of pH on the photocatalytic degradation of amoxicillin, the experiment was carried out in the pH range of 3–11. Removal efficiency was highest at pH 9 due to the concentrated hydroxyl radicals in the solution. These radicals play a significant role in oxidizing organic contaminants. The enhanced degradation efficiency of pharmaceuticals in alkaline conditions may be due to two facts: the formation of a large amount of hydroxyl radical at a high pH due to the availability of OH^- on the surface of the catalyst that can easily be oxidized to form hydroxyl radicals and the hydrolysis of the pharmaceuticals due to the instability of the β-lactam ring at large pH values [34]. Furthermore, the dissolution of the nanoparticle was more noticeable at a low pH value, which could moderately explain the lower AMX removal at a lower pH in addition to limited generation of hydroxyl radicals [53].

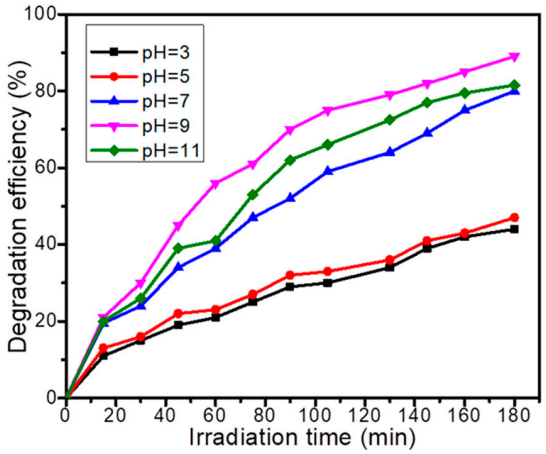

Figure 4. Effect of pH on photocatalytic degradation of amoxicillin (C_0 = 15 mg/L, catalyst dose = 1 g/L).

3.4.2. Pollutant Initial Concentration

Effect of initial concentration of AMX on the photocatalytic degradation efficiency is displayed in Figure 5. Various degradation experiments were conducted by changing the concentration from 5 to 50 mg/L. Degradation efficiency was increased first with increasing concentration of AMX to 15 mg/L, and then decreased beyond this concentration. The presumed reason for the decrement is that when the concentration of AMX increases, large amount of AMX molecules adsorb on the surface of the photocatalyst and cause inhibitive effect on the reaction of AMX with h^+ and/or ·OH, as a result of absence of any direct contact between AMX and the charge carriers [54]. Moreover, the AMX molecules also absorb the light and the photons could not reach the surface of the photocatalyst; hence degradation efficiency diminishes [55].

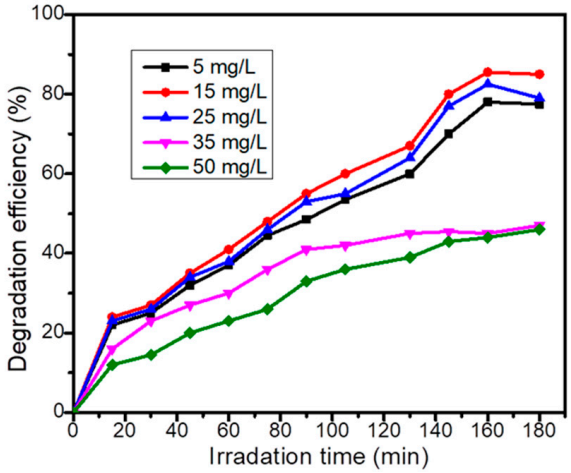

Figure 5. Effect of initial concentration of amoxicillin on photocatalytic degradation (pH = 9, catalyst dose = 1 g/L).

3.4.3. Catalyst Dose

Catalyst amount added into aqueous solution is one of the important parameters influencing photocatalytic performance. To optimize the catalyst load for obtaining maximum degradation efficiency, different amounts of the catalyst in the range 0.5–2.5 g/L were dispersed into the amoxicillin solution. As represented in Figure 6, maximum degradation efficiency of AMX was observed at 1 g/L catalyst dosage. Degradation efficiency was improved as catalyst amount increased to 1 g/L, beyond that the effect was less marked. Increasing the amount of catalyst enhances the number of photons absorbed on the surface of the catalyst. Thus, the active sites and the light penetration into the solution also increase which in turn improved the e^-/h^+ pair generation and increased the amount of OH radicals and the number of organic pollutant adsorbed on the surface. As a result, generation of electron/hole pairs and reactive OH radicals on the photocatalyst surface were increased, which enhanced the oxidation of AMX. However, when the catalyst dosage is excess, degradation efficiency decreases due to collision of active molecules with basic state molecules losing their activity. Furthermore, it should be pronounced that the decrement in degradation efficiency at a higher amount of catalyst may be also associated with improved scattering and turbidity effects, which inhibit the penetration of light into the surface of particles. On the other hand, particle–particle agglomeration results in the reduction of active sites on the surface of catalyst [56].

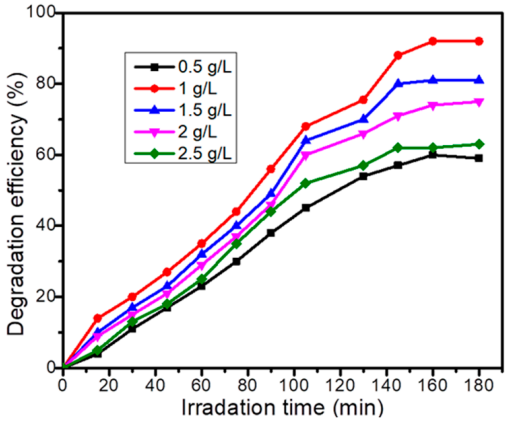

Figure 6. Effect of catalyst dose on photocatalytic degradation of amoxicillin (C0 = 15 mg/L, pH = 9).

3.4.4. Photocatalytic Degradation of Amoxicillin under the Optimum Conditions

After optimizing the pH 9.0, catalyst dose 1 g/L, and AMX initial concentration 15 mg/L, the photocatalytic degradation of the antibiotic was carried out using pure Cu_2O and Mn-doped Cu_2O nanoparticles. As shown in Figure 7, the degradation efficiency of AMX reached 65% and 92% using Cu_2O and Mn-doped Cu_2O respectively within 180 min irradiation time. Despite the crystallite size of the as-synthesized photocatalyst, Mn-doped Cu_2O exhibited enhanced degradation efficiency than Cu_2O nanoparticles; this might be due to narrow band gap energy and unfeasibility of electron–hole recombination in Mn-doped Cu_2O [57]. When a semiconductor is illuminated by light, electrons are excited to the conduction band and holes are present in the valence band. Overall, after a few micro seconds the e^- and h^+ recombine. The metal dopant traps electron from the conduction band of the semiconductor, hence hindering the recombination of electron/hole pair. As the metal dopant traps large number of electrons, large amount of superoxide radical anions ($O_2^{\cdot -}$) are formed. The generation of large number of superoxide radical anions is important for attacking the organic pollutant which in turn enhances the degradation efficiency [58]. Therefore, Mn delays the rapid recombination by increasing the electron–hole separation. Moreover, crystal defects can create states in the energy level of Cu_2O; these states can absorb sub-band gap photons which increase light harvesting by the material. Tamam et al. [59] reported photocatalytic degradation of Rh–B dye using Mn-doped CuO nanostructured material under visible light irradiation. According to the authors, Mn-doped CuO has better photocatalytic performance in mineralization of Rh–B dye than CuO, with 93.8% dye mineralization compared to 56.52% for CuO. The Mn-doped CuO has faster charge transport but negligible electron-hole recombination than the un-doped CuO. In our study, 65% and 92% of amoxicillin was removed using pristine Cu_2O and Mn-doped Cu_2O nanoparticles respectively, which is comparable with the previous work reported by Tamam et al. (2022). Photocatalytic degradation of amoxicillin was studied by [34] using TiO_2 photocatalyst under UV irradiation. According to the authors, 60% of amoxicillin was degraded within 300 min of irradiation. Rani et al. (2021) examined the photocatalytic degradation of amoxicillin using TiO_2-SiO_2 composites. 88% of amoxicillin was degraded in 150 min under UV light illumination [35]. The researchers used UV light as energy source, but sunlight was used in our work. Photocatalytic degradation of methyl blue using Cu_2O prepared using plant extract has been reported by Kerour et al. [38]. The average size of these particles ranged between 24 and 61 nm, as proved by XRD analysis, while 37–40 nm in our present study. The band gap of Cu_2O reported by Kerour was in the range of 2.50 eV to 2.62 eV which is higher than the band gap of the present study, 2.2 to 2.3. According to Kerour et al. (2018), nearly 70% of methyl blue was degraded in the presence of Cu_2O after 3 min exposure to visible light. Methyl blue was completely removed after 10 min irradiation in visible light. The photocatalytic degradation result reported by Kerour is a little different from our result.

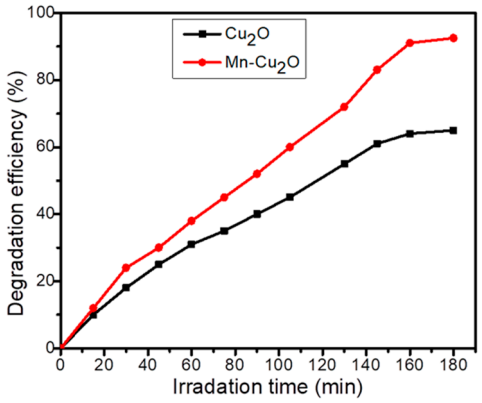

Figure 7. Photocatalytic degradation of amoxicillin using Cu_2O and Mn-Cu_2O under the optimal conditions (pH = 9, C0 = 15 mg/L and amount of catalysts = 1 g/L).

3.5. Kinetic Study

Kinetics of the photocatalytic degradation of amoxicillin by the pure and Mn-doped Cu_2O nanoparticle was investigated using pseudo-first-order and pseudo-second-order kinetics as depicted in Figure 8. The linear form of the pseudo-first-order kinetic model is written below.

$$ln\frac{C0}{Ct} = k_1 t$$

where C_t is the concentration of AMX at time t, C_0 is the initial concentration of AMX, k_1 is pseudo-first-order rate constant, and t is time. The plots of $\ln(C_0/C_t)$ versus time gave a straight line with a slope of k_1. Besides the pseudo-first-order equation, the linear form of pseudo second order kinetic is as described below.

$$\frac{1}{Ct} - \frac{1}{C0} = k_2 t$$

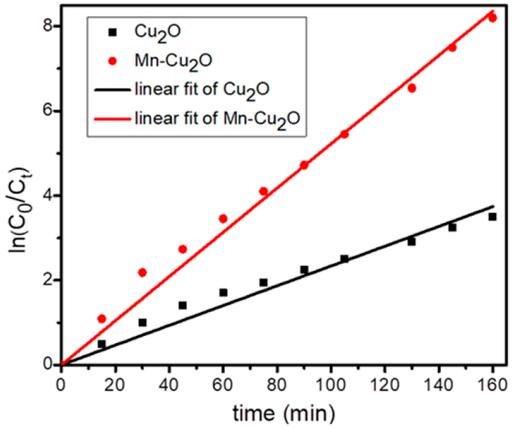

Figure 8. Plot of $\ln(C_0/C)$ versus t.

The plots of $1/C_t - 1/C_0$ versus time gave a straight line with a slope of k_2 [60]. Based on the acquired data, higher correlation coefficients R^2 were obtained in the pseudo-first-order kinetic model. Consequently, the photocatalytic degradation of AMX using the undoped and Mn-doped Cu_2O nanoparticle is best fitted to pseudo-first-order kinetics [61]. The rate constant (k) values of the undoped and Mn-doped Cu_2O were found to be 0.033 and 0.073 min^{-1} respectively for AMX degradation. A good correlation coefficient value, R^2 of 0.984 and 0.995 was acquired for the pure and Mn-doped Cu_2O nanoparticles. Based on the reaction constants, the Mn-doped Cu_2O nanoparticle is a better photocatalyst than the undoped, which is in agreement with the photocatalytic activity study.

3.6. Proposed Mechanism

Figure 9 displays the mechanism for enhanced photocatalytic activity of Mn-doped Cu_2O under sunlight radiations. When a photocatalyst irradiates by light, excitation of electrons from valence band to conduction band and formation of holes in valence band take place. Generally, after a few micro seconds they recombine. Upon irradiating Mn-doped Cu_2O with sunlight, the photogenerated electrons migrate from the valence band of Cu_2O to the conduction band, while producing same amount of holes in the valence band. Because the Mn-Cu_2O new Fermi level is lower than the conduction band of Cu_2O, the photogenerated electrons migrate from the conduction band of Cu_2O to the Mn. Therefore, Mn serves as an electron trap to hinder the electron–hole recombination. The electrons on the surface of Mn then react with the adsorbed oxygen to form superoxide radical anions ($O_2^{\cdot -}$). Simultaneously, the valence band holes of cuprous oxide react with water to form highly reactive hydroxyl radicals (·OH). The formation of a large amount of $O_2^{\cdot -}$ and ·OH is important for attacking the organic molecules. After producing $O_2^{\cdot -}$, Mn^+ receives an electron from Cu_2O and becomes Mn [62]. The valence band (E_{VB}) and conduction band (E_{CB}) potential values of Mn-doped Cu_2O and Cu_2O were found to be +2 eV and −0.2 eV respectively as shown in Figure 9 [63–65].

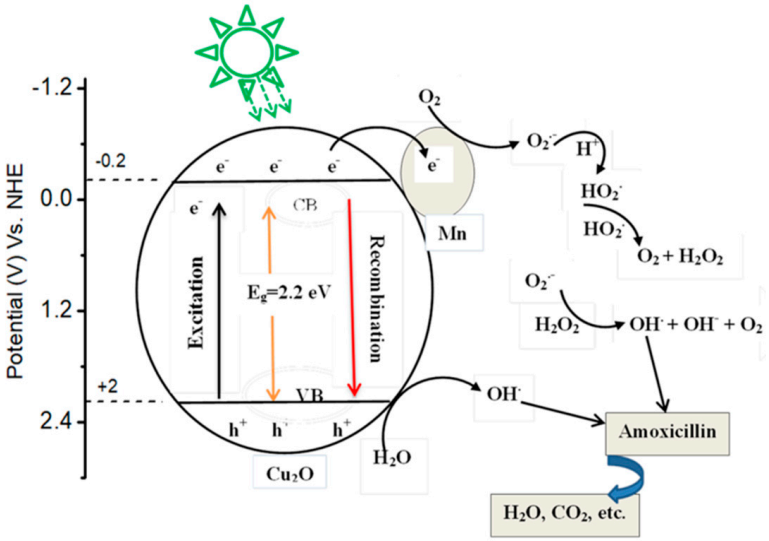

Figure 9. Proposed mechanism for the photocatalytic degradation of amoxicillin using Mn-doped Cu_2O nanoparticles under solar light irradiation.

4. Conclusions

In this paper, undoped and Mn-doped Cu_2O photocatalyst were synthesized using aloe vera leaves extract in an eco-friendly approach. The photocatalytic degradation of amoxicillin depends on catalyst dose, pH, and initial concentration of pollutant. Mn-doped Cu_2O photocatalyst exhibited a big enhancement in activity compared to the bare Cu_2O. This enhancement could be due to visible light harvesting and strong inhibition of electron–hole recombination. The mechanism under sunlight irradiation reveals that the Mn is used to trap an electron and increases electron–hole separation. Based on the findings, Mn-doped Cu_2O is a potential photocatalyst for the removal of pharmaceuticals from wastewater.

Author Contributions: Y.T.G. took part in conceptualization, methodology, formal analysis, original draft preparation, manuscript preparation, sorting and data analysis, investigation and validation. S.M.Y. was responsible for collecting resources and supervision. Z.G.K. took part in visualization and project administration. All authors have read and agreed to the published version of the manuscript.

Funding: This research was funded by Werabe University grant number WRU1213, 2020 and the APC was partially funded by this University. The rest of the APC was covered by the authors.

Data Availability Statement: The data used to support the results of this article such as XRD, SEM, UV-Vis, and photocatalytic degradation data can be found from the corresponding author upon request.

Acknowledgments: The authors are grateful to the Werabe University for funding the work with grant number WRU1213, 2020.

Conflicts of Interest: The authors declare that there are no conflict of interest associated with the work reported in this paper.

References

1. Pezoti, O.; Cazetta, A.L.; Bedin, K.C.; Souza, L.S.; Martins, A.C.; Silva, T.L.; Júnior, O.O.S.; Visentainer, J.V.; Almeida, V.C. NaOH-activated carbon of high surface area produced from guava seeds as a high-efficiency adsorbent for amoxicillin removal: Kinetic, isotherm and thermodynamic studies. *Chem. Eng. J.* **2016**, *288*, 778–788. [CrossRef]
2. Pouretedal, H.; Sadegh, N. Effective removal of amoxicillin, cephalexin, tetracycline and penicillin G from aqueous solutions using activated carbon nanoparticles prepared from vine wood. *J. Water Process Eng.* **2014**, *1*, 64–73. [CrossRef]
3. Moussavi, G.; Alahabadi, A.; Yaghmaeian, K.; Eskandari, M. Preparation, characterization and adsorption potential of the NH4Cl-induced activated carbon for the removal of amoxicillin antibiotic from water. *Chem. Eng. J.* **2013**, *217*, 119–128. [CrossRef]
4. Olama, N.; Dehghani, M.; Malakootian, M. The removal of amoxicillin from aquatic solutions using the TiO_2/UV-C nanophotocatalytic method doped with trivalent iron. *Appl. Water Sci.* **2018**, *8*, 1–12. [CrossRef]
5. Ahmadi, M.; Motlagh, H.R.; Jaafarzadeh, N.; Mostoufi, A.; Saeedi, R.; Barzegar, G.; Jorfi, S. Enhanced photocatalytic degradation of tetracycline and real pharmaceutical wastewater using MWCNT/TiO2 nano-composite. *J. Environ. Manag.* **2017**, *186*, 55–63. [CrossRef]
6. Chaba, J.M.; Nomngongo, P.N. Effective adsorptive removal of amoxicillin from aqueous solutions and wastewater samples using zinc oxide coated carbon nanofiber composite. *Emerg. Contam.* **2019**, *5*, 143–149. [CrossRef]
7. Yu, F.; Li, Y.; Han, S.; Ma, J. Adsorptive removal of antibiotics from aqueous solution using carbon materials. *Chemosphere* **2016**, *153*, 365–385. [CrossRef]
8. Balarak, D.; Mostafapour, F.; Bazrafshan, E.; Saleh, T.A. Studies on the adsorption of amoxicillin on multi-wall carbon nanotubes. *Water Sci. Technol.* **2017**, *75*, 1599–1606. [CrossRef]
9. Kanakaraju, D.; Kockler, J.; Motti, C.A.; Glass, B.D.; Oelgemöller, M. Titanium dioxide/zeolite integrated photocatalytic adsorbents for the degradation of amoxicillin. *Appl. Catal. B Environ.* **2015**, *166*, 45–55. [CrossRef]
10. Serna-Galvis, E.A.; Ferraro, F.; Silva-Agredo, J.; Torres-Palma. Degradation of highly consumed fluoroquinolones, penicillins and cephalosporins in distilled water and simulated hospital wastewater by UV254 and UV254/persulfate processes. *Water Res.* **2017**, *122*, 128–138. [CrossRef]
11. Elmolla, E.S.; Chaudhuri, M. Degradation of amoxicillin, ampicillin and cloxacillin antibiotics in aqueous solution by the UV/ZnO photocatalytic process. *J. Hazard. Mater.* **2010**, *173*, 445–449. [CrossRef] [PubMed]
12. Zuccato, E.; Castiglioni, S.; Bagnati, R.; Melis, M.; Fanelli, R. Source, occurrence and fate of antibiotics in the Italian aquatic environment. *J. Hazard. Mater.* **2010**, *179*, 1042–1048. [CrossRef] [PubMed]
13. Klavarioti, M.; Mantzavinos, D.; Kassinos, D. Removal of residual pharmaceuticals from aqueous systems by advanced oxidation processes. *Environ. Int.* **2009**, *35*, 402–417. [CrossRef] [PubMed]
14. Andreozzi, R.; Caprio, V.; Insola, A.; Marotta, R. Advanced oxidation processes (AOP) for water purification and recovery. *Catal. Today* **1999**, *53*, 51–59. [CrossRef]
15. Ong, C.B.; Ng, L.Y.; Mohammad, A.W. A review of ZnO nanoparticles as solar photocatalysts: Synthesis, mechanisms and applications. *Renew. Sustain. Energy Rev.* **2018**, *81*, 536–551. [CrossRef]
16. Gad-Allah, T.A.; Ali, M.E.; Badawy, M.I. Photocatalytic oxidation of ciprofloxacin under simulated sunlight. *J. Hazard. Mater.* **2011**, *186*, 751–755. [CrossRef] [PubMed]
17. Kudo, A.; Miseki, Y. Heterogeneous photocatalyst materials for water splitting. *Chem. Soc. Rev.* **2009**, *38*, 253–278. [CrossRef]
18. Mousavi-Kamazani, M.; Zarghami, Z.; Rahmatolahzadeh, R.; Ramezani, M. Solvent-free synthesis of Cu-Cu_2O nanocomposites via green thermal decomposition route using novel precursor and investigation of its photocatalytic activity. *Adv. Powder Technol.* **2017**, *28*, 2078–2086. [CrossRef]
19. Yu, Y.; Du, F.P.; Jimmy, C.Y.; Zhuang, Y.Y.; Wong, P.K. One-dimensional shape-controlled preparation of porous Cu_2O nanowhiskers by using CTAB as a template. *J. Solid State Chem.* **2004**, *177*, 4640–4647. [CrossRef]
20. Yang, J.; Li, Z.; Zhao, C.; Wang, Y.; Liu, X. Facile synthesis of Ag–Cu2O composites with enhanced photocatalytic activity. *Mater. Res. Bull.* **2014**, *60*, 530–536. [CrossRef]
21. Wang, T.; Wei, Y.; Chang, X.; Li, C.; Li, A.; Liu, S.; Zhang, J.; Gong, J. Homogeneous Cu2O pn junction photocathodes for solar water splitting. *Appl. Catal. B Environ.* **2018**, *226*, 31–37. [CrossRef]
22. Zhang, W.; Ma, Y.; Yang, Z.; Tang, X.; Li, X.; He, G.; Cheng, Y.; Fang, Z.; He, R.; Zhang, Y. Analysis of synergistic effect between graphene and octahedral cuprous oxide in cuprous oxide-graphene composites and their photocatalytic application. *J. Alloy. Compd.* **2017**, *712*, 704–713. [CrossRef]

23. Kusmierek, E.; Mierczynski, P.; Kedziora, A.; Nowosielska, M.; Maniukiewicz, W.; Vorobyov, S.; Vitkovskaya, R.; Maniecki, T.P. Photocatalytic degradation of an azo dye over novel monometallic copper catalysts supported on fibreglass. *Catal. Lett.* **2017**, *147*, 2448–2461. [CrossRef]
24. Ravichandran, A.T.; Dhanabalan, K.; Ravichandran, K.; Mohan, R.; Karthika, K.; Vasuhi, A.; Muralidharan, B. Tuning the Structural and Optical Properties of SILAR-Deposited Cu 2 O Films Through Zn Doping. *Acta Metall. Sin.* **2015**, *28*, 1041–1046. [CrossRef]
25. Kumar, A.; Kumar, A.; Sharma, G.; Ala'a, H.; Naushad, M.; Ghfar, A.A.; Stadler, F.J. Quaternary magnetic BiOCl/g-C_3N_4/Cu_2O/Fe_3O_4 nano-junction for visible light and solar powered degradation of sulfamethoxazole from aqueous environment. *Chem. Eng. J.* **2018**, *334*, 462–478. [CrossRef]
26. Deng, Y.; Tang, L.; Zeng, G.; Feng, C.; Dong, H.; Wang, J.; Feng, H.; Liu, Y.; Zhou, Y.; Pang, Y. Plasmonic resonance excited dual Z-scheme $BiVO_4$/Ag/Cu_2O nanocomposite: Synthesis and mechanism for enhanced photocatalytic performance in recalcitrant antibiotic degradation. *Environ. Sci. Nano* **2017**, *4*, 1494–1511. [CrossRef]
27. Xia, Y.; He, Z.; Hu, K.; Tang, B.; Su, J.; Liu, Y.; Li, X. Fabrication of n-$SrTiO_3$/p-Cu_2O heterojunction composites with enhanced photocatalytic performance. *J. Alloy. Compd.* **2018**, *753*, 356–363. [CrossRef]
28. Cheng, L.; Tian, Y.; Zhang, J. Construction of pn heterojunction film of Cu2O/α-Fe2O3 for efficiently photoelectrocatalytic degradation of oxytetracycline. *J. Colloid Interface Sci.* **2018**, *526*, 470–479. [CrossRef]
29. Christopher, P.; Ingram, D.B.; Linic, S. Enhancing photochemical activity of semiconductor nanoparticles with optically active Ag nanostructures: Photochemistry mediated by Ag surface plasmons. *J. Phys. Chem. C* **2010**, *114*, 9173–9177. [CrossRef]
30. Song, J.Y.; Kim, B.S. Rapid biological synthesis of silver nanoparticles using plant leaf extracts. *Bioprocess Biosyst. Eng.* **2009**, *32*, 79–84. [CrossRef]
31. Chandran, S.P.; Chaudhary, M.; Pasricha, R.; Ahmad, A.; Sastry, M. Synthesis of gold nanotriangles and silver nanoparticles using Aloevera plant extract. *Biotechnol. Prog.* **2006**, *22*, 577–583. [CrossRef] [PubMed]
32. Ijaz, I.; Gilani, E.; Nazir, A.; Bukhari, A. Detail review on chemical, physical and green synthesis, classification, characterizations and applications of nanoparticles. *Green Chem. Lett. Rev.* **2020**, *13*, 223–245. [CrossRef]
33. Malhotra, S.P.K.; Alghuthaymi, M.A. Biomolecule-assisted biogenic synthesis of metallic nanoparticles. In *Agri-Waste and Microbes for Production of Sustainable Nanomaterials*; Elsevier: Amsterdam, The Netherlands, 2022; pp. 139–163.
34. Elmolla, E.S.; Chaudhuri, M. Photocatalytic degradation of amoxicillin, ampicillin and cloxacillin antibiotics in aqueous solution using UV/TiO2 and UV/H2O2/TiO2 photocatalysis. *Desalination* **2010**, *25*, 46–52. [CrossRef]
35. Rani, S.; Garg, A.; Singh, N. Photocatalytic degradation and mineralization of amoxicillin and ofloxacin using TiO_2-SiO_2 composites. *Toxicol. Environ. Chem.* **2021**, *103*, 137–153. [CrossRef]
36. Mohammadi, R.; Massoumi, B.; Rabani, M. Photocatalytic decomposition of amoxicillin trihydrate antibiotic in aqueous solutions under UV irradiation using Sn/TiO_2 nanoparticles. *Int. J. Photoenergy* **2012**, *2012*, 514856. [CrossRef]
37. Rao, K.G.; Ashok, C.H.; Rao, K.V.; Chakra, C.S.; Tambur, P. Green synthesis of TiO_2 nanoparticles using Aloe vera extract. *Int. J. Adv. Res. Phys. Sci.* **2015**, *2*, 28–34.
38. Kerour, A.; Boudjadar, S.; Bourzami, R.; Allouche, B. Eco-friendly synthesis of cuprous oxide (Cu_2O) nanoparticles and improvement of their solar photocatalytic activities. *J. Solid State Chem.* **2018**, *263*, 79–83. [CrossRef]
39. Sharma, R.; Patel, S.; Pargaien, K. Synthesis, characterization and properties of Mn-doped ZnO nanocrystals. *Adv. Nat. Sci.: Nanosci. Nanotechnol.* **2012**, *3*, 035005. [CrossRef]
40. Jiang, Y.; Sun, Y.; Liu, H.; Zhu, F.; Yin, H. Solar photocatalytic decolorization of CI Basic Blue 41 in an aqueous suspension of TiO_2–ZnO. *Dye. Pigment.* **2008**, *78*, 77–83. [CrossRef]
41. Balarak, D.; Mostafapour, F.K. Photocatalytic degradation of amoxicillin using UV/Synthesized NiO from pharmaceutical wastewater. *Indones. J. Chem.* **2019**, *19*, 211–218. [CrossRef]
42. Yu, X.; Zhang, J.; Zhang, J.; Niu, J.; Zhao, J.; Wei, Y.; Yao, B. Photocatalytic degradation of ciprofloxacin using Zn-doped Cu_2O particles: Analysis of degradation pathways and intermediates. *Chem. Eng. J.* **2019**, *374*, 316–327. [CrossRef]
43. Downs, R.T.; Hall-Wallace, M. The American Mineralogist crystal structure database. *Am. Mineral.* **2003**, *88*, 247–250.
44. Achouri, F.; Corbel, S.; Balan, L.; Mozet, K.; Girot, E.; Medjahdi, G.; Said, M.B.; Ghrabi, A.; Schneider, R. Porous Mn-doped ZnO nanoparticles for enhanced solar and visible light photocatalysis. *Mater. Des.* **2016**, *101*, 309–316. [CrossRef]
45. Sun, S.; Zhang, X.; Yang, Q.; Liang, S.; Zhang, X.; Yang, Z. Cuprous oxide (Cu_2O) crystals with tailored architectures: A comprehensive review on synthesis, fundamental properties, functional modifications and applications. *Prog. Mater. Sci.* **2018**, *96*, 111–173. [CrossRef]
46. Juang, F.-R.; Chern, W.-C. Octahedral Cu_2O nanoparticles decorated by silver catalyst for high sensitivity nonenzymatic H2O2 detection. *Mater. Sci. Semicond. Process.* **2019**, *101*, 156–163. [CrossRef]
47. Norouzi, A.; Nezamzadeh-Ejhieh, A.; Fazaeli, R. A Copper (I) oxide-zinc oxide nano-catalyst hybrid: Brief characterization and study of the kinetic of its photodegradation and photomineralization activities toward methylene blue. *Mater. Sci. Semicond. Process.* **2021**, *122*, 105495. [CrossRef]
48. Li, J.; Sun, L.; Yan, Y.; Zhu, Z. One-step in-situ fabrication of silver-modified Cu_2O crystals with enhanced visible photocatalytic activity. *Micro Nano Lett.* **2016**, *11*, 363–365. [CrossRef]

49. Bordbar, M.; Jafari, S.; Yeganeh-Faal, A.; Khodadadi, B. Influence of different precursors and Mn doping concentrations on the structural, optical properties and photocatalytic activity of single-crystal manganese-doped ZnO. *J. Iran. Chem. Soc.* **2017**, *14*, 897–906. [CrossRef]
50. Tichy, L.; Ticha, H. Interrelation between the photo-induced shift of the optical band gap and Urbach/exponential edge slope in a-Se. *J. Non-Cryst. Solids* **2019**, *515*, 113–115. [CrossRef]
51. Mallesham, B.; Roy, S.; Bose, S.; Nair, A.N.; Sreenivasan, S.; Shutthanandan, V.; Ramana, C.V. Crystal chemistry, band-gap red shift, and electrocatalytic activity of iron-doped gallium oxide ceramics. *ACS Omega* **2019**, *5*, 104–112. [CrossRef]
52. Zhao, H.; Pan, F.; Li, Y. A review on the effects of TiO2 surface point defects on CO_2 photoreduction with H_2O. *J. Mater.* **2017**, *3*, 17–32. [CrossRef]
53. Zyoud, A.H.; Zorba, T.; Helal, M.; Zyoud, S.; Qamhiya, N.; Hajamohideen, A.R.; Zyoud, S.; Hilal, H.S. Direct sunlight-driven degradation of 2-chlorophenol catalyzed by kaolinite-supported ZnO. *Int. J. Environ. Sci. Technol.* **2019**, *16*, 6267–6276. [CrossRef]
54. Sahel, K.; Perol, N.; Chermette, H.; Bordes, C.; Derriche, Z.; Guillard, C. Photocatalytic decolorization of Remazol Black 5 (RB5) and Procion Red MX-5B—Isotherm of adsorption, kinetic of decolorization and mineralization. *Appl. Catal. B: Environ.* **2007**, *77*, 100–109. [CrossRef]
55. Asahi, R.Y.O.J.I.; Morikawa, T.A.K.E.S.H.I.; Ohwaki, T.; Aoki, K.; Taga, Y. Visible-light photocatalysis in nitrogen-doped titanium oxides. *Science* **2001**, *293*, 269–271. [CrossRef] [PubMed]
56. Çağlar Yılmaz, H.; Akgeyik, E.; Bougarrani, S.; El Azzouzi, M.; Erdemoğlu, S. Photocatalytic degradation of amoxicillin using Co-doped TiO2 synthesized by reflux method and monitoring of degradation products by LC–MS/MS. *J. Dispers. Sci. Technol.* **2020**, *41*, 414–425. [CrossRef]
57. Ashebir, M.E.; Tesfamariam, G.M.; Nigussie, G.Y.; Gebreab, T.W. Structural, optical, and photocatalytic activities of Ag-doped and Mn-doped ZnO nanoparticles. *J. Nanomater.* **2018**, *2018*, 9425938. [CrossRef]
58. Welderfael, T.; Pattabi, M.; Pattabi, R.M. Photocatalytic activity of Ag-N co-doped ZnO nanorods under visible and solar light irradiations for MB degradation. *J. Water Process Eng.* **2016**, *14*, 117–123. [CrossRef]
59. Tamam, N.; Aadil, M.; Hassan, W.; Ejaz, S.R.; Najm, Z.M.; Alsafari, I.A.; Aman, S.; Trukhanov, A.V.; Al-Buriahi, M.S.; Boukhris, I. Surfactant assisted synthesis of nanostructured Mn-doped CuO: An efficient photocatalyst for environmental remediation. *Ceram. Int.* **2022**, *48*, 29589–29600. [CrossRef]
60. Kakavandi, B.; Takdastan, A.; Jaafarzadeh, N.; Azizi, M.; Mirzaei, A.; Azari, A. Application of Fe3O4@ C catalyzing heterogeneous UV-Fenton system for tetracycline removal with a focus on optimization by a response surface method. *J. Photochem. Photobiol. A Chem.* **2016**, *314*, 178–188. [CrossRef]
61. Safari, G.H.; Hoseini, M.; Seyedsalehi, M.; Kamani, H.; Jaafari, J.; Mahvi, A.H. Photocatalytic degradation of tetracycline using nanosized titanium dioxide in aqueous solution. *Int. J. Environ. Sci. Technol.* **2015**, *12*, 603–616. [CrossRef]
62. Qin, H.; Wei, Q.; Wu, J.; Yang, F.; Zhou, B.; Wang, Y.; Tian, S. Effects of Ag nanoparticles on the visible-light-driven photocatalytic properties of Cu_2O nanocubes. *Mater. Chem. Phys.* **2019**, *232*, 240–245. [CrossRef]
63. Wang, R.; Xie, X.; Xu, C.; Lin, Y.; You, D.; Chen, J.; Li, Z.; Shi, Z.; Cui, Q.; Wang, M. Bi-piezoelectric effect assisted ZnO nanorods/PVDF-HFP spongy photocatalyst for enhanced performance on degrading organic pollutant. *Chem. Eng. J.* **2022**, *439*, 135787. [CrossRef]
64. Xie, X.; Wang, R.; Ma, Y.; Chen, J.; Shi, Z.; Cui, Q.; Li, Z.; Xu, C. Sulfate-Functionalized Core–Shell ZnO/CdS/Ag_2S Nanorod Arrays with Dual-Charge-Transfer Channels for Enhanced Photoelectrochemical Performance. *ACS Appl. Energy Mater.* **2022**, *5*, 6228–6237. [CrossRef]
65. Xie, X.; Wang, R.; Ma, Y.; Chen, J.; Cui, Q.; Shi, Z.; Li, Z.; Xu, C. Photothermal-Effect-Enhanced Photoelectrochemical Water Splitting in MXene-Nanosheet-Modified ZnO Nanorod Arrays. *ACS Appl. Nano Mater.* **2022**, *5*, 11150–11159. [CrossRef]